CHEMISTRY OF MATERIALS

pubs.acs.org/cm

Article

Microwave-Assisted Synthesis of the New Solid-Solution $(V_{1-x}Cr_x)_2GaC$ ($0 \leq x \leq 1$), a Pauli Paramagnet Almost Matching the Stoner Criterion for $x = 0.80$

Niels Kubitza, Ruiwen Xie, Ivan Tarasov, Chen Shen, Hongbin Zhang, Ulf Wiedwald, and Christina S. Birkel*

Cite This: *Chem. Mater.* 2023, 35, 4427−4434

Read Online

ACCESS | Metrics & More | Article Recommendations | Supporting Information

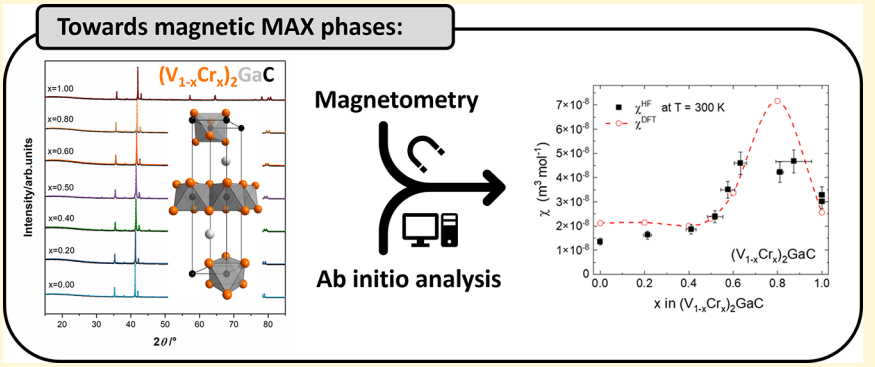

ABSTRACT: MAX phases that exhibit long-range magnetic order in the bulk are still very hard to synthesize. Chromium and manganese are the cutoff elements when transitioning through the 3dmetals that still form stable full and doped MAX phases, respectively. An iron-based (on the *M*-site) bulk MAX phase does not exist. Therefore, other strategies to induce long-range magnetic ordering in bulk MAX phases are necessary to open the path to new functional materials. Here, we demonstrate the nonconventional synthesis of a hitherto unknown MAX phase solid-solution $(V_{1-x}Cr_x)_2GaC$ by microwave heating. The full series with $0 < x < 1$ ($x = 0.20, 0.40, 0.50, 0.60, 0.80$) forms almost single phase with minimal differences in their morphology. Their magnetic properties, however, differ rather significantly, with a maximum susceptibility around $x = 0.80$. Both the experimental and theoretical/ab initio magnetic analysis confirm that the solid-solution $(V_{1-x}Cr_x)_2GaC$ is an itinerant Pauli paramagnet that almost fulfills the Stoner criterion for ferromagnetic order (for compositions with x around 0.80). This is a powerful insight into how chemical composition couples with electronic structure and the resulting bulk magnetic properties because it provides crucial guidelines to produce long-range ordered magnetic MAX phases.

INTRODUCTION

One of the key synthetic approaches to tailor, improve, or discover materials with remarkable properties is to dope or mix elements with a different electronic structure into an already existing system. This has been proven in various materials classes, such as magnetic[1−3] and semiconductor materials,[4−6] ceramics,[7−9] and the so-called MAX phases.[10−13] The latter are hexagonally layered (space group $P6_3/mmc$) ternary transition metal carbides, nitrides, and carbonitrides with the general sum formula $M_{n+1}AX_n$ (n = 1, 2, 3 (4,[14] 5[15])), where M is an (early-to-mid) transition metal, A is a main group element mostly of groups 13 and 14, and X is carbon and/or nitrogen. A combination of weak $M-A$ bonds, strong $M-X$ bonds, and the layered crystal structure enable their unique characteristic to combine metallic (e.g., electrical and thermal conductivity), as well as ceramic properties (e.g., oxidation and corrosion resistance) within one substance class.[16,17] This makes them potentially interesting as structural materials for high-temperature applications, such as protective coatings.[18] Since the first synthesis-based reports attributed to MAX phases by Kudielka[19] and Nowotny et al.[20−24] in the 1960s, more than 150 MAX phases are known to date.[16] In particular, the substantial work by Barsoum et al.,[17] who discovered the outstanding set of properties[25] and coined the name "MAX phases," has laid the foundation for today's interest in the respective substance class. Over the recent years, the strong increase in the exploration of new MAX phases has been

Received: March 16, 2023
Revised: May 2, 2023
Published: May 17, 2023

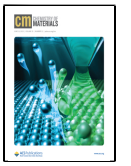

heavily driven by the preparation of solid-solution phases, resulting in a significant broadening of the initial property profile. For instance, magnetic properties have been induced by incorporating magnetic elements (Mn, Fe) on the *M*-site. This approach was first conducted in 2013 by Ingason et al., with the synthesis of $(Cr_{0.75}Mn_{0.25})_2GeC$ thin films exhibiting long-range magnetic ordering.[26] In the same year, Ingason et al. reported the synthesis of Mn_2GaC thin films,[27] the first MAX phase with manganese as the sole *M*-element. The latter revealed ferromagnetic characteristics up to 230 K with potential toward spintronics or magnetocaloric applications.[27,28] Since then, in both thin-film and bulk synthesis approaches, many doping studies with manganese on the *M*-site have been reported. As parent phases, predominantly chromium-based (Cr_2AC) phases with *A* = Al,[13,29] Ga,[11,30] and Ge[26,31] were studied. However, particularly bulk approaches have faced the problem of competing side phases leading to only small Mn amounts that can be incorporated into the MAX phase structure (e.g., $(Cr_{0.94}Mn_{0.06})_2AlC$,[32] $(Cr_{1-x}Mn_x)_2GeC$; $x \leq 0.25$[33]). Additionally, the interpretation of the magnetic characterization is due to the inherent nanolaminated character being very complex and surpasses traditional considerations of magnetism.[34] In order to circumvent several disadvantages of conventional bulk approaches (e.g., long reaction times, bad energy efficiency, stabilization of other thermodynamically stable phases),[35,36] nonconventional methods, such as microwave heating or sol−gel synthesis were used to synthesize Mn- and Fe-doped 211 phases (e.g., $(Cr_{1-x}M_x)_2AC$; *M* = Fe,[13] Mn;[11,13] A = Al,[13] Ga[11]). Nonetheless, these syntheses could not produce magnets with high ordering temperatures similar to Mn_2GaC films either. Alternative studies extended the "conventional" approaches to dope Mn or Fe on the *M*-site and focused on rare earth elements, leading to so-called ordered MAX phases.[37,38] Furthermore, the modification of the *A*-site was considered as a promising approach. The synthesis of $V_2(Sn_{1-x}M_x)C$[39] *M* = Mn, Fe, Co, Ni or the so-called *A*-element replacement successfully exchanges the *A*-sites, where, e.g., aluminum is replaced by iron using iron-based Lewis acids.[40,41] On the other hand, in systems where gallium acts as the sole *A*-element, magnetic studies are mainly limited to the manganese *M*-site doping of the 211 phase Cr_2GaC phase.[11,30,32] For V_2GaC in general, to the best of our knowledge, no *M*-site solid solutions have been reported yet. In the vanadium-based bulk system, magnetic studies are restricted to the phases with aluminum as the *A*-element (e.g., $(V_{1-x}Mn_x)_2AlC$)[42] and the investigated Cr/V-solid solution on the *M*-site is also only reported for the aluminum-based phases.[43,44] For the latter, no magnetic characterization has been conducted so far.

By concentrating on the less investigated group of gallium-based MAX phases, we are adding a new member to the MAX phase family with the synthesis of the hitherto unknown solid-solution MAX phase $(V_{1-x}Cr_x)_2GaC$ $(0 \leq x \leq 1)$ using the rapid microwave heating synthesis technique. Herewith, we are introducing a new approach within the field of magnetic MAX phases to first optimize the paramagnetic properties of a MAX phase system before focusing on further doping studies toward magnetically ordered phases. All obtained materials were characterized by means of powder X-ray diffraction (XRD), electron microscopy (SEM), and magnetometry (VSM). In addition, ab initio calculations were performed to elucidate the strongly stoichiometric-dependent magnetic behavior of the samples.

EXPERIMENTAL SECTION

For the syntheses of the parent phases V_2GaC and Cr_2GaC, as well as solid-solution phases $(V_{1-x}Cr_x)_2GaC$ (x = 0.20, 0.40, 0.50, 0.60, 0.80), the elemental precursor amounts were based on 0.5 g of the desired product. A detailed summary of the used precursor amounts can be found in the Supporting Information (Table SI-1). Initially, gallium flakes (Alfa Aesar, >99%) were cut under atmospheric conditions and subsequently transferred into an argon-filled glovebox. Chromium (Sigma-Aldrich, 99%, ∼325 mesh), vanadium (Alfa Aesar, 99.5%, ∼325 mesh), and carbon (Alfa Aesar, >99.9%, APS 2−15 μm) powders were thoroughly mixed using an agate mortar. The mixture was then loosely mixed with the cut gallium flakes and pressed into a dense pellet (d = 10 mm, 3 t, 10 s). All pellets were subsequently sealed into an evacuated fused silica ampoule, which was placed into 7 g of activated charcoal (Grüssing, 2.5 mm) acting as a susceptor material and annealed inside a microwave oven (CEM, MARS6) following a defined temperature program (Table SI-2). Prior to further characterization steps, the pellets were finely ground (<100 μm (Figure SI-3)) using an agate mortar and stored under atmospheric conditions.

CHARACTERIZATION

X-ray powder diffraction data were obtained using a Stadi P (Stoe & Cie GmbH) with monochromatized Cu Kα radiation (λ = 1.540596 Å) and the Mythen 1K (Dectris) detector in transmission geometry at room temperature. For measurements, small sample amounts were deposited between X-ray amorphous adhesive film (Scotch) on a flat sample holder and rotated orthogonally to the X-ray source. Rietveld refinements were performed using the program TOPAS (Bruker). First, based on the respective structural models, the side phase amounts in wt % were determined before a detailed refinement of the lattice parameters was conducted based on the Le Bail method.

SEM images were taken at the XL30 FEG (Philips) using an acceleration voltage of 25 kV adapted with an APOLLO X-SDD detector (EDAX) for collecting EDX data. The EDX data was evaluated using the software EDAX GENESIS.

Magnetic properties were studied by vibrating sample magnetometry (VSM) in a PPMS DynaCool system (Quantum Design). Dried powder (20−50 mg) was weighed and put into polymer capsules. Measurements were taken within the field range of ±9 T at variable temperatures ranging from 3 to 400 K.

The ab initio calculations of the magnetic susceptibility were performed in the fully relativistic regime using the SPR-KKR package,[45,46] which utilizes the linear response theory on the basis of the Green's function technique. The *k*-mesh convergence for both self-consistent and magnetic susceptibility calculations was carefully tested, and a *k*-mesh of 17 × 17 × 3 was adopted. The cutoff l_{max} = 3 was selected for the angular momentum expansion of Green's function, and the generalized gradient approximation (GGA (PBE)) was adopted for the exchange−correlation functional. $(V_{1-x}Cr_x)_2GaC$ alloys were simulated with the experimentally measured lattice parameters using the coherent potential approximation (CPA),[47] in which V and Cr were assumed to be chemically disordered on the *M*-sites.

RESULTS AND DISCUSSION

Structural Analysis. Starting from the parent phase V_2GaC, the amount of chromium was nominally increased in steps of 20 atom % (except for the additional sample with 50 atom %) until the second parent phase Cr_2GaC was obtained.

https://doi.org/10.1021/acs.chemmater.3c00591
Chem. Mater. 2023, 35, 4427−4434

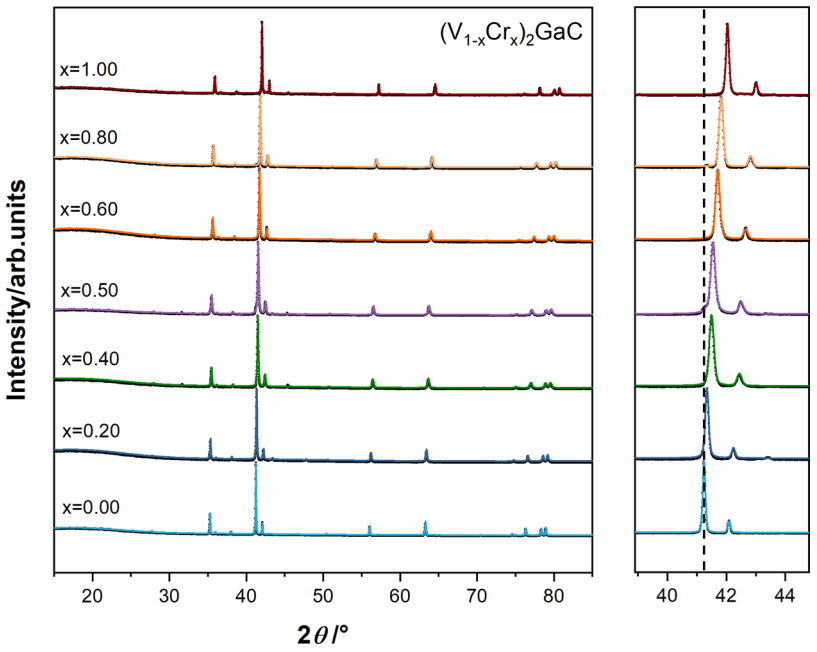

Figure 1. Le Bail refinements (colored lines) of the X-ray powder diffraction data of the solid-solution phase $(V_{1-x}Cr_x)_2GaC$ (black dots) based on the structural model of V_2GaC[48] providing the space group *P*63/*mmc*. *x* was nominally increased in steps of 20 atom % (except for 50 atom %).

Table 1. Summary of the Extracted Lattice Parameters of the Solid-Solution $(V_{1-x}Cr_x)_2GaC$ Based on Le Bail Refinements, with the Respective Errors Shown in Parentheses

nominal composition	actual composition	*a*-lattice parameter, Å	*c*-lattice parameter, Å	cell volume, Å^3
V_2GaC	V_2GaC	2.9371(3)	12.8752(2)	96.19(2)
$(V_{0.80}Cr_{0.20})_2GaC$	$(V_{0.80}Cr_{0.20})_2GaC$	2.9302(5)	12.8268(3)	95.38(4)
$(V_{0.60}Cr_{0.40})_2GaC$	$(V_{0.59}Cr_{0.41})_2GaC$	2.9205(7)	12.7676(3)	94.31(5)
$(V_{0.50}Cr_{0.50})_2GaC$	$(V_{0.52}Cr_{0.48})_2GaC$	2.9160(7)	12.7442(4)	93.85(5)
$(V_{0.40}Cr_{0.60})_2GaC$	$(V_{0.37}Cr_{0.63})_2GaC$	2.9088(6)	12.7173(3)	93.19(5)
$(V_{0.20}Cr_{0.80})_2GaC$	$(V_{0.19}Cr_{0.81})_2GaC$	2.8999(5)	12.6589(3)	92.19(4)
Cr_2GaC	Cr_2GaC	2.8845(5)	12.6062(3)	90.84(4)

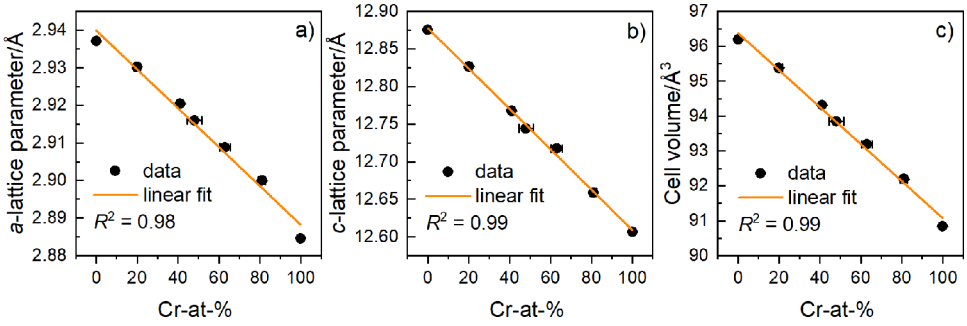

Figure 2. Graphical illustration of the dependency between both the *a*-lattice parameters (a), *c*-lattice parameters (b), the cell volumes (c), and the actual atomic % of chromium including error bars, including simple linear fit (orange lines).

As shown in the refined X-ray powder diffraction data (Figure 1), V_2GaC was obtained single phase, whereas Cr_2GaC revealed small amounts of Cr_3Ga (0.3 wt %) and $CrGa_4$ (1.8 wt %) side phases. All solid-solution samples were obtained nearly single phase with $CrGa_3$ (1.3 wt % for x = 0.20) and $CrGa_4$ (2.8 wt % for x = 0.40; 1.7 wt % for x = 0.50) as assignable side phases.

By increasing the amount of chromium, a monotonous peak shift toward higher 2θ angles is observed, which is in accordance with the smaller atomic radius of chromium (2.33 Å) compared to vanadium (2.52 Å),[49] following Vegard's law.[50]

In order to extract the lattice parameters of all studied MAX phases (Table 1), Le Bail refinements were performed based on the structural model of V_2GaC[48] with space group *P*63/*mmc*. A detailed summary of the refinements can be found in the Supporting Information (Tables SI-3−SI-9). The lattice parameters of the parent phases V_2GaC and Cr_2GaC are in good agreement with those reported in the literature.[48,51] In accordance with the 2θ peak shift toward higher diffraction angles, the lattice parameters and cell volumes of the solid-

https://doi.org/10.1021/acs.chemmater.3c00591
Chem. Mater. 2023, 35, 4427−4434

solution phases (Table 1) exhibit an almost linear decrease toward Cr_2GaC. A graphical illustration of this trend is visualized in Figure 2, where *a*- and *c*-lattice parameters, as well as cell volumes, are plotted against the actual averaged amount of vanadium (atom %) determined via EDX analysis (Figure SI-2 and Tables SI-10−SI-14). The latter are in good agreement with the nominal compositions. In addition, a simple linear regression of the data validates the approximate linear behavior with R^2 values close to 1 (R^2 (*a*-lattice) = 0.98; R^2 (*c*-lattice) = 0.99; R^2 (cell volumes) = 0.99). This in turn also confirms Vegard's law, which describes the linear dependency of the lattice parameters and the percentual composition of the solid-solution phase.[50]

SEM micrographs (Figure 3) reveal the typical morphology of the samples, which can be described as a mixture of the

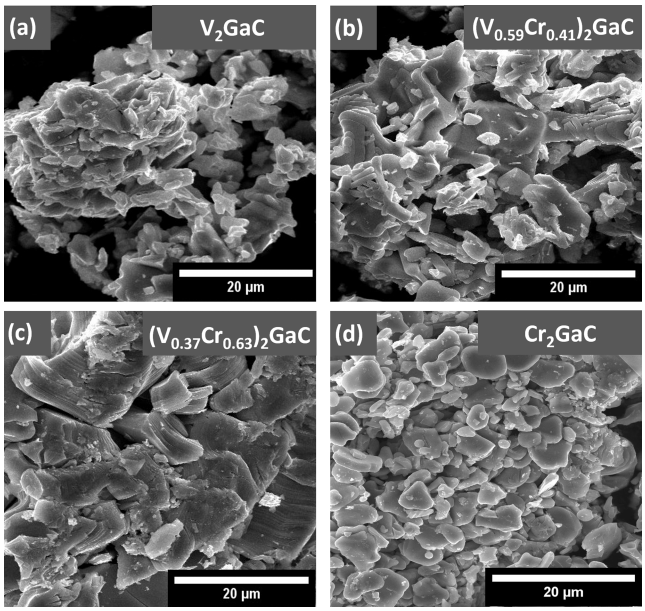

Figure 3. SEM micrographs showing the typical morphology of V_2GaC (a), $(V_{0.59}Cr_{0.41})_2GaC$ (b), $(V_{0.37}Cr_{0.63})_2GaC$ (c), and Cr_2GaC (d), respectively, representing the nonconventionally synthesized solid-solution system $(V_{1-x}Cr_x)_2GaC$ ($0 \le x \le 1$).

characteristic anisotropic MAX phase layered structures combined with surfaces, partially covered with drop-like particles and finer substructures. Here, the two parent compounds V_2GaC and Cr_2GaC, as well as $(V_{0.59}Cr_{0.41})_2GaC$ and $(V_{0.37}Cr_{0.63})_2GaC$ were chosen as representative examples for the entire system $(V_{1-x}Cr_x)_2GaC$ ($0 \le x \le 1$). In general, no meaningful dependency of the morphology on the Cr/V ratio was observed, and the morphologies are very similar. Further micrographs of the other members of the solid-solution system can be found in Figure SI-4.

Magnetic Analysis. The magnetic response of the $(V_{1-x}Cr_x)_2GaC$ ($0 \le x \le 1$) system is presented in Figure 4. As a representative of the full series, the field-dependent magnetization of the $(V_{0.37}Cr_{0.63})_2GaC$ powder sample is strictly linear at T = 300 K, indicating paramagnetism. At lower temperatures, a slight nonlinearity sets in, as shown in Figure 4a. The small absolute magnetization at 9 T is below 0.2 $Am^2 kg^{-1}$ at T = 3 K and only about 50% larger than the magnetization at 300 K. Such small variations point to temperature-independent Pauli paramagnetism of the conduction electrons, as observed before for the Cr_2GaC MAX phase.[52] The nonlinear response, however, can be ascribed to tiny amounts of impurity phases not visible in the X-ray diffraction data, which is an often-observed complication in the characterization of paramagnetic MAX phases.[13,52] The remanent magnetization of the $(V_{0.37}Cr_{0.63})_2GaC$ sample is 4 × 10^{-3} $Am^2 kg^{-1}$ at T = 3 K, decreasing with increasing temperature and a factor of 50 lower than the paramagnetic response of the MAX phase at large fields. Assuming a typical saturation magnetization of 10 $Am^2 kg^{-1}$ or more of a ferromagnetic impurity phase means that the sample is essentially phase pure and the phase content of the ferromagnetic impurity is maximally 0.04%. Such amounts are not detectable by structural methods but significant as add-ons in magnetometry.

Both the small temperature dependence of the MAX phase magnetic response and an add-on component at smallest amounts also show up in the zero-field cooling (ZFC) and field cooling (FC) curves in B = 10 mT, as presented in Figure 4b for the $(V_{0.48}Cr_{0.52})_2GaC$ and $(V_{0.59}Cr_{0.41})_2GaC$ samples, respectively. Both samples show almost constant magnetization values at T = 300 K and above. The $(V_{0.48}Cr_{0.52})_2GaC$ sample magnetization gradually increases with decreasing temperature, while below T = 15 K, a steep reduction is observed. ZFC/FC of the $(V_{0.59}Cr_{0.41})_2GaC$ sample splits at 230 K, indicating a ferromagnetic side phase. However, the differences remain small as compared to the constant paramagnetic offset. The data shown in Figure 4a,b is representative of all the sample series. At low temperatures, deviations from a constant positive value, as expected for Pauli paramagnetism, are observed due to tiny amounts of side phases. Thus, in the following, we restrict the data analysis to higher temperatures at which the traces of paramagnetic or ferromagnetic impurities have the lowest contribution to the signals.

Figure 3c shows the magnetization as a function of temperature in the largest available field of B = 9 T in the interval 300−400 K. The numbers Cr_x on the right reflect the composition of the $(V_{1-x}Cr_x)_2GaC$ samples. First, it is striking that the magnetization is almost temperature-independent, further indicating Pauli paramagnetism. Following the different stoichiometries, the values rise from V_2GaC to x = 0.63, saturating to a plateau up to x = 0.87 and decrease again for Cr_2GaC. Since Pauli paramagnetism is dominant at 300−400 K in these samples, the signals point toward an enhanced density of states at the Fermi level E_F. This becomes clearer in Figure 4d showing the magnetic susceptibility as extracted from linear fits of the field-dependent magnetization in the interval $|B|$ = 6−9 T at T = 300 K. This high-field susceptibility χ is strictly constant, as also shown in Figure 4a by the linear response for $(V_{0.37}Cr_{0.63})_2GaC$. The error bars reflect the stoichiometry scattering as determined by SEM-EDX and the uncertainty of the susceptibilities for the ordinate and the abscissa, respectively. Between x = 0.6 and 0.9, an enhanced susceptibility is obtained that is 4 times larger than for V_2GaC and 50% increased as compared to Cr_2GaC.

Summarizing the magnetic data, all samples of the $(V_{1-x}Cr_x)_2GaC$ MAX phases system for $0 < x < 1$ are Pauli paramagnets. At low temperatures, trace amounts appear as add-on signals. From 300 to 400 K, we obtain almost constant magnetic susceptibilities, which, however, vary up to 400% as a function of stoichiometry. Note that the magnetic energy splitting of spin-up and spin-down states of the conduction electrons at the Fermi level is much smaller at B = 9 T (meV) than the Fermi energy (several eV). At this point, one is

https://doi.org/10.1021/acs.chemmater.3c00591
Chem. Mater. 2023, 35, 4427−4434

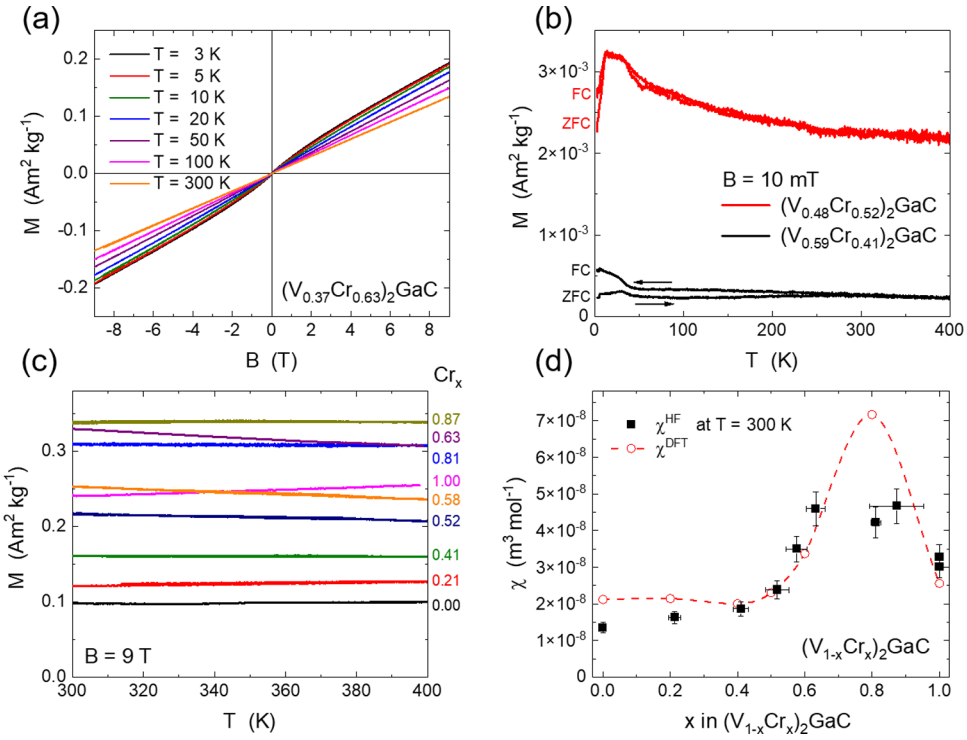

Figure 4. Magnetic properties of the $(V_{1-x}Cr_x)_2GaC$ solid-solution system. (a) Field-dependent magnetization of the $(V_{0.37}Cr_{0.63})_2GaC$ sample at various temperatures between 3 and 300 K. (b) Zero-field cooling and field cooling curves in B = 10 mT for the $(V_{0.48}Cr_{0.52})_2GaC$ and $(V_{0.59}Cr_{0.41})_2GaC$ samples. (c) Temperature-dependent magnetization of all solid-solution samples. Numbers on the right indicate the x in $(V_{1-x}Cr_x)_2GaC$. (d) Magnetic susceptibility from the field-dependent magnetization in $(V_{1-x}Cr_x)_2GaC$ samples at 300 K. The susceptibility is extracted from a linear fitting of the signal in the interval $|B|$ = 6−9 T. Circles indicate the DFT-calculated magnetic susceptibility. The line is a guide to the eye.

tempted to use the Pauli relation $\chi = \chi_P = \mu_0\mu_B^2 D(E_F)$ to determine the density of states at the Fermi level. While for V_2AlC[42] and Cr_2GaC,[53] this works reasonably, in the present case, the increased susceptibility for $0.63 < x < 0.87$ leads to extremely large numbers $D(E_F)$ appearing unrealistic at first glance. Thus, we decided to extract the susceptibility directly from DFT calculations and compare it with experiments. The results are shown in Figure 4d and will be discussed in the following.

Theoretical Calculations. Overall, the magnetic susceptibilities derived from magnetometry and DFT calculations (Figure 4d) agree well with respect to the Cr concentration. In both cases, the same trend with a nonlinear behavior and a maximum susceptibility at around x = 0.80 is observed. Except for the nominal composition of x = 0.80, the experimentally derived magnetic susceptibilities exhibit only small deviations in comparison to the calculated ones. In order to exclude systematic mistakes, the preparation and magnetic characterization of $(V_{0.20}Cr_{0.80})_2GaC$ have been conducted twice following the same method, however, with no further convergence to the calculated values. Sample information of the latter can be found in the Supporting Information (Figure SI-5 and Tables SI-15 and SI-16).

The element-resolved V and Cr contributions to the magnetic susceptibilities are shown in Figure 5. The total magnetic susceptibility χ_{tot} is composed of the total spin susceptibility, which is a sum of the spin susceptibility χ_s, including the spin−orbit coupling (SOC) induced spin susceptibility, the total Van Vleck orbital susceptibility χ_o, which includes the enhanced orbital susceptibility and the SOC-induced orbital susceptibility, and finally the diamagnetic

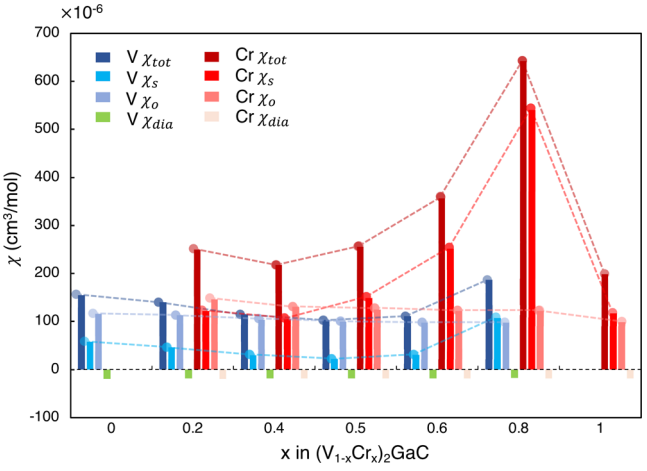

Figure 5. Element-resolved total magnetic susceptibility (χ_{tot}), total spin susceptibility (χ_s), total Van Vleck orbital susceptibility (χ_o), and diamagnetic susceptibility (χ_{dia}) as a function of Cr doping x in $(V_{1-x}Cr_x)_2GaC$.

susceptibility χ_{dia} consisting of core and band contributions. As it can be obviously seen in Figure 5, the total spin susceptibility of Cr is responsible for the peak at x = 0.80 in the $(V_{1-x}Cr_x)_2GaC$ MAX phase system, while χ_o and χ_{dia} are insensitive to the change of Cr content.

Such a nonlinear dependence of the spin susceptibility on the Cr concentration can be understood based on the Stoner theory.[54] The obtained Stoner parameter I, the nonmagnetic density of states (DOS) at the Fermi level per atom $n(E_F)$, the

https://doi.org/10.1021/acs.chemmater.3c00591
Chem. Mater. 2023, 35, 4427−4434

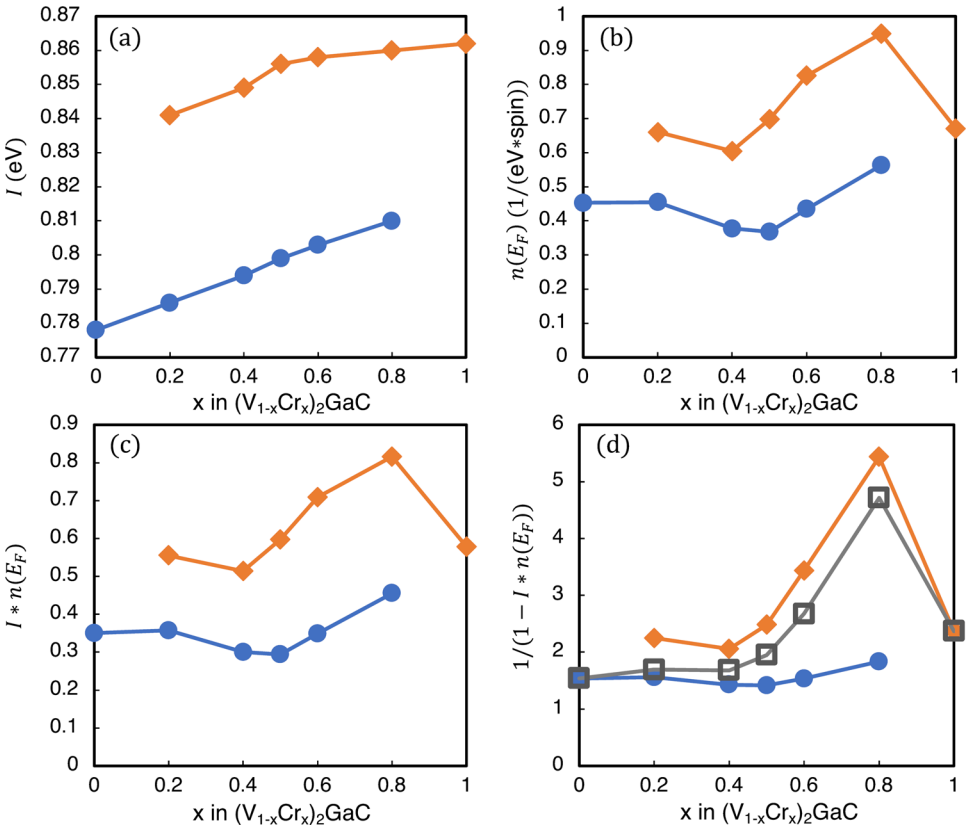

Figure 6. (a) Stoner parameter I, (b) density of states at Fermi level $n(E_F)$ per atomic site, (c) product of I and $n(E_F)$, and (d) Stoner enhancement parameter $(1 - I{\cdot}n(E_F))^{-1}$ as a function of Cr doping x in $(V_{1-x}Cr_x)_2GaC$ MAX phases. Blue lines with circles and orange lines with diamonds denote the corresponding parameters for V and Cr, respectively. In panel (d), the gray line with squares represents the Stoner enhancement parameter averaged with respect to the V and Cr contents.

product of I and $n(E_F)$, and the Stoner enhancement parameter $(1 - I{\cdot}n(E_F))^{-1}$ are plotted in Figure 5 as a function of the Cr content x. As is well known, the Stoner parameter I is a quasi-atomic property, which can be slightly tuned by the chemical effects.[54] For bcc V and Cr, the Stoner parameters[54] are around 0.71 and 0.76 eV, respectively, which are close to the calculated values in the current work, being ~0.78 eV for V_2GaC and 0.86 eV for Cr_2GaC. As demonstrated in Figure 6b,c, $n(E_F)$ and $I{\cdot}n(E_F)$ display apparently analogous trends for the variation of magnetic susceptibility with the Cr content, indicating that the magnetic response of the $(V_{1-x}Cr_x)_2GaC$ MAX phase system is in the itinerant regime. We note that the maximum $I{\cdot}n(E_F)$ is about 0.82 for x = 0.80, which is smaller than 1, resulting in no magnetic long-range order in these systems. Correspondingly, the susceptibility can be formulated as $\chi = \chi_0{\cdot}(1 - I{\cdot}n(E_F))^{-1}$, where χ_0 is the Pauli susceptibility, and the Stoner enhancement parameter $(1 - I{\cdot}n(E_F))^{-1}$ can reproduce the dependence of the susceptibility on the chemical composition. Therefore, both the experimentally derived magnetic susceptibilities and the theoretical calculations have proven that the $(V_{1-x}Cr_x)_2GaC$ MAX phase system is a prototypical itinerant paramagnet, which is nearly magnetically ordered. Increasing the density of states $n(E_F)$ further around x = 0.80, e.g., by Mn doping, can lead to overcoming the Stoner criterion of long-range magnetic order. Alternatively, two-dimensional MXene materials can shape the density of states further.

CONCLUSIONS

In this work, we have demonstrated the synthesis of a new gallium-containing MAX phase solid-solution $(V_{1-x}Cr_x)_2GaC$ $(0 \le x \le 1)$ using the microwave-assisted heating technique. The solid solution exhibits no miscibility gap, and the refined lattice parameters almost perfectly follow Vegard's law. SEM micrographs show that the composition of the phases has no influence on the typical MAX phase-like morphology of the bulk compounds. On the other hand, the magnetic behavior of the phases is highly dependent on the composition. VSM measurements revealed that all samples are Pauli paramagnets; however, the obtained susceptibilities vary nonlinear up to 400%, with a maximum at x = 0.80. By considering the Stoner theory, ab initio calculations confirm the experimental magnetic data and identify the $(V_{1-x}Cr_x)_2GaC$ system as a prototypical itinerant paramagnet which is nearly magnetically ordered ($I{\cdot}n(E_F)$ = 0.82). Overall, these findings provide a necessary starting point for the challenging synthesis of new magnetically ordered MAX phases.

ASSOCIATED CONTENT

Supporting Information

The Supporting Information is available free of charge at https://pubs.acs.org/doi/10.1021/acs.chemmater.3c00591.

Additional synthesis parameters, refinement results from X-ray diffraction, scanning electron micrographs, and elemental analysis (PDF)

https://doi.org/10.1021/acs.chemmater.3c00591
Chem. Mater. 2023, 35, 4427−4434

AUTHOR INFORMATION

Corresponding Author

Christina S. Birkel − *Department of Chemistry, Technische Universität Darmstadt, 64287 Darmstadt, Germany; School of Molecular Sciences, Arizona State University, Tempe, Arizona 85282, United States;* orcid.org/0000-0001-8979-5214; Email: Christina.Birkel@asu.edu

Authors

Niels Kubitza − *Department of Chemistry, Technische Universität Darmstadt, 64287 Darmstadt, Germany*

Ruiwen Xie − *Institute of Materials Science, Technische Universität Darmstadt, 64287 Darmstadt, Germany*

Ivan Tarasov − *Faculty of Physics and Center for Nanointegration Duisburg-Essen, University of Duisburg-Essen, 47057 Duisburg, Germany*

Chen Shen − *Institute of Materials Science, Technische Universität Darmstadt, 64287 Darmstadt, Germany;* orcid.org/0000-0002-8538-9873

Hongbin Zhang − *Institute of Materials Science, Technische Universität Darmstadt, 64287 Darmstadt, Germany*

Ulf Wiedwald − *Faculty of Physics and Center for Nanointegration Duisburg-Essen, University of Duisburg-Essen, 47057 Duisburg, Germany;* orcid.org/0000-0002-3209-4078

Complete contact information is available at: https://pubs.acs.org/10.1021/acs.chemmater.3c00591

Author Contributions

The manuscript was written through contributions of all authors. All authors have given approval to the final version of the manuscript.

Funding

This work has been supported by the Deutsche Forschungsgemeinschaft (DFG, German Research Foundation) within CRC/TRR 270, projects B03 and B02, A05 (Project-ID 405553726).

Notes

The authors declare no competing financial interest.

REFERENCES

(1) Kim, A. S. Magnetic Properties of NdDyFeCoAlB Alloys. *J. Appl. Phys.* **1988**, *63*, 3975.

(2) Rehman, S. U.; Jiang, Q.; He, L.; Xiong, H.; Liu, K.; Wang, L.; Yang, M.; Zhong, Z. Microstructure and Magnetic Properties of NdFeB Alloys by Co-Doping Alnico Elements. *Phys. Lett. A* **2019**, *383*, No. 125878.

(3) Rehman, S. U.; Liu, H.; Zhong, S.; Liang, H.; Liu, R.; Jiang, Q.; Yang, M.; Zhong, Z. Retaining the Curie Temperature of Ce Substituted Nd-Fe-B Nano-Ribbons by Alnico Elements Substitution. *Intermetallics* **2022**, *141*, No. 107428.

(4) Haraguchi, K.; Katsuyama, T.; Hiruma, K.; Ogawa, K. GaAs P-n Junction Formed in Quantum Wire Crystals. *Appl. Phys. Lett.* **1992**, *60*, 745.

(5) Persson, C.; Zhao, Y.-J.; Lany, S.; Zunger, A. N-Type Doping of $CuInSe_2$ and $CuGaSe_2$. *Phys. Rev. B* **2005**, *72*, No. 035211.

(6) Lany, S.; Zhao, Y.-J.; Persson, C.; Zunger, A. Halogen N-Type Doping of Chalcopyrite Semiconductors. *Appl. Phys. Lett.* **2005**, *86*, 042109.

(7) Takahashi, S. Effects of Impurity Doping in Lead Zirconate-Titanate Ceramics. *Ferroelectrics* **1982**, *41*, 143−156.

(8) Pereira, M.; Peixoto, A. G.; Gomes, M. J. M. Effect of Nb Doping on the Microstructural and Electrical Properties of the PZT Ceramics. *J. Eur. Ceram. Soc.* **2001**, *21*, 1353−1356.

(9) Hou, J.; Kumar, R. V.; Qu, Y.; Krsmanovic, D. B-Site Doping Effect on Electrical Properties of $Bi_4Ti_{3-2x}Nb_xTa_xO_{12}$ Ceramics. *Scr. Mater.* **2009**, *61*, 664−667.

(10) Lin, S.; Huang, Y.; Zu, L.; Kan, X.; Lin, J.; Song, W.; Tong, P.; Zhu, X.; Sun, Y. Alloying Effects on Structural, Magnetic, and Electrical/Thermal Transport Properties in MAX-Phase $Cr_{2-x}M_xGeC$ (M = Ti, V, Mn, Fe, and Mo). *J. Alloys Compd.* **2016**, *680*, 452−461.

(11) Siebert, J. P.; Mallett, S.; Juelsholt, M.; Pazniak, H.; Wiedwald, U.; Page, K.; Birkel, C. S. Structure Determination and Magnetic Properties of the Mn-Doped MAX Phase Cr_2GaC. *Mater. Chem. Front.* **2021**, *5*, 6082−6091.

(12) Azzouz-Rached, A.; Rached, H.; Ouadha, I.; Rached, D.; Reggad, A. The Vanadium-Doping Effect on Physical Properties of the Zr_2AlC MAX Phase Compound. *Mater. Chem. Phys.* **2021**, *260*, No. 124189.

(13) Hamm, C. M.; Bocarsly, J. D.; Seward, G.; Kramm, U. I.; Birkel, C. S. Non-Conventional Synthesis and Magnetic Properties of MAX Phases $(Cr/Mn)_2AlC$ and $(Cr/Fe)_2AlC$. *J. Mater. Chem. C* **2017**, *5*, 5700−5708.

(14) Deysher, G.; Shuck, C. E.; Hantanasirisakul, K.; Frey, N. C.; Foucher, A. C.; Maleski, K.; Sarycheva, A.; Shenoy, V. B.; Stach, E. A.; Anasori, B.; Gogotsi, Y. Synthesis of Mo4VAlC4 MAX Phase and Two-Dimensional Mo_4VC_4 MXene with Five Atomic Layers of Transition Metals. *ACS Nano* **2020**, *14*, 204−217.

(15) Lin, Z.; Zhuo, M.; Zhou, Y.; Li, M.; Wang, J. Microstructures and Theoretical Bulk Modulus of Layered Ternary Tantalum Aluminum Carbides. *J. Am. Ceram. Soc.* **2006**, *89*, 3765−3769.

(16) Sokol, M.; Natu, V.; Kota, S.; Barsoum, M. W. On the Chemical Diversity of the MAX Phases. *Trends Chem.* **2019**, *1*, 210−223.

(17) Barsoum, M. W. The $M_{N+1}AX_N$ Phases: A New Class of Solids. *Prog. Solid State Chem.* **2000**, *28*, 201−281.

(18) Gonzalez-Julian, J. Processing of MAX Phases: From Synthesis to Applications. *J. Am. Ceram. Soc.* **2021**, *104*, 659−690.

(19) Kudielka, H.; Rohde, H. Strukturuntersuchungen an Carbosulfiden von Titan Und Zirkon. *Z. Kristallogr.* **1960**, *114*, 447−456.

(20) Jeitschko, W.; Nowotny, H.; Benesovsky, F. Die H-Phasen Ti_2TlC, Ti_2PbC, Nb_2InC, Nb_2SnC Und Ta_2GaC. *Monatsh. Chem.* **1964**, *95*, 431−435.

(21) Jeitschko, W.; Nowotny, H.; Benesovsky, F. Ternäre Carbide Und Nitride in Systemen: Übergangsmetall-Metametall-Kohlenstoff (Stickstoff). *Monatsh. Chem.* **1964**, *95*, 156−157.

(22) Jeitschko, W.; Nowotny, H.; Benesovsky, F. Die H-Phasen: Ti_2CdC, Ti_2GaC, Ti_2GaN, Ti_2InN, Zr_2InN Und Nb_2GaC. *Monatsh. Chem.* **1964**, *95*, 178−179.

(23) Jeitschko, W.; Nowotny, H.; Benesovsky, F. Kohlenstoffhaltige Ternäre Verbindungen (H-Phase). *Monatsh. Chem.* **1963**, *94*, 672−676.

(24) Jeitschko, W.; Nowotny, H.; Benesovsky, F. Kohlenstoffhaltige Ternäre Verbindungen (V-Ge-C, Nb-Ga-C, Ta-Ga-C, Ta-Ge-C, Cr-Ga-C Und Cr-Ge-C). *Monatsh. Chem.* **1963**, *94*, 844−850.

(25) Barsoum, M. W.; El-Raghy, T. *Synthesis and Characterization of a Remarkable Ceramic: Ti_3SiC_2*; John Wiley & Sons, Ltd., 1996; Vol. *79*, pp 1953−1956.

(26) Ingason, A. S.; Mockute, A.; Dahlqvist, M.; Magnus, F.; Olafsson, S.; Arnalds, U. B.; Alling, B.; Abrikosov, I. A.; Hjörvarsson, B.; Persson, P. O. Å.; Rosen, J. Magnetic Self-Organized Atomic Laminate from First Principles and Thin Film Synthesis. *Phys. Rev. Lett.* **2013**, *110*, No. 195502.

(27) Ingason, A. S.; Petruhins, A.; Dahlqvist, M.; Magnus, F.; Mockute, A.; Alling, B.; Hultman, L.; Abrikosov, I. A.; Persson, P. O. Å.; Rosen, J. A Nanolaminated Magnetic Phase: Mn_2GaC. *Mater. Res. Lett.* **2013**, *2*, 89−93.

(28) Novoselova, I. P.; Petruhins, A.; Wiedwald, U.; Ingason, Á. S.; Hase, T.; Magnus, F.; Kapaklis, V.; Palisaitis, J.; Spasova, M.; Farle, M.; Rosen, J.; Salikhov, R. Large Uniaxial Magnetostriction with Sign Inversion at the First Order Phase Transition in the Nanolaminated Mn_2GaC MAX Phase. *Sci. Rep.* **2018**, *8*, No. 2637.

(29) Sobolev, K.; Pazniak, H.; Farle, M.; Rodionova, V.; Wiedwald, U. Synthesis, Phase Purification and Magnetic Characterization of the $(Cr_{1-x}Mn_x)_2AlC$ MAX-Phase. *J. Mater. Chem. C* **2021**, *9*, 16516−16522.
(30) Petruhins, A.; Ingason, A. S.; Lu, J.; Magnus, F.; Olafsson, S.; Rosen, J. Synthesis and Characterization of Magnetic $(Cr_{0.5}Mn_{0.5})_2GaC$ Thin Films. *J. Mater. Sci.* **2015**, *50*, 4495−4502.
(31) Rivin, O.; Caspi, E. N.; Pesach, A.; Shaked, H.; Hoser, A.; Georgii, R.; Tao, Q.; Rosen, J.; Barsoum, M. W. Evidence for Ferromagnetic Ordering in the MAX Phase $(Cr_{0.96}Mn_{0.04})_2GeC$. *Mater. Res. Lett.* **2017**, *5*, 465−471.
(32) Mockute, A.; Lu, J.; Moon, E. J.; Yan, M.; Anasori, B.; May, S. J.; Barsoum, M. W.; Rosen, J. Solid Solubility and Magnetism upon Mn Incorporation in the Bulk Ternary Carbides Cr_2AlC and Cr_2GaC. *Mater. Res. Lett.* **2015**, *3*, 16−22.
(33) Liu, Z.; Waki, T.; Tabata, Y.; Nakamura, H. Mn-Doping-Induced Itinerant-Electron Ferromagnetism in Cr_2GeC. *Phys. Rev. B* **2014**, *89*, No. 054435.
(34) Ingason, A. S.; Dahlqvist, M.; Rosén, J. Magnetic MAX Phases from Theory and Experiments; a Review. *J. Phys.: Condens. Matter* **2016**, *28*, No. 433003.
(35) Groh, M. F.; Heise, M.; Kaiser, M.; Ruck, M. Sanfte Festkörperchemie. *Nachr. Chem.* **2013**, *61*, 26−29.
(36) Siebert, J. P.; Hamm, C. M.; Birkel, C. S. Microwave Heating and Spark Plasma Sintering as Non-Conventional Synthesis Methods to Access Thermoelectric and Magnetic Materials. *Appl. Phys. Rev.* **2019**, *6*, 041314.
(37) Tao, Q.; Lu, J.; Dahlqvist, M.; Mockute, A.; Calder, S.; Petruhins, A.; Meshkian, R.; Rivin, O.; Potashnikov, D.; Caspi, E. N.; et al. Atomically Layered and Ordered Rare-Earth i-MAX Phases: A New Class of Magnetic Quaternary Compounds. *Chem. Mater.* **2019**, *31*, 2476−2485.
(38) Petruhins, A.; Lu, J.; Hultman, L.; Rosen, J. Synthesis of Atomically Layered and Chemically Ordered Rare-Earth (RE) i-MAX Phases;$(Mo_{2/3}RE_{1/3})_2GaC$ with RE= Gd, Tb, Dy, Ho, Er, Tm, Yb, and Lu. *Mater. Res. Lett.* **2019**, *7*, 446−452.
(39) Li, Y.; Lu, J.; Li, M.; Chang, K.; Zha, X.; Zhang, Y.; Chen, K.; Persson, P. O. Å.; Hultman, L.; Eklund, P.; Du, S.; Francisco, J. S.; Chai, Z.; Huang, Z.; Huang, Q. Multielemental Single−Atom-Thick A Layers in Nanolaminated $V_2(Sn, A)$ C (A = Fe, Co, Ni, Mn) for Tailoring Magnetic Properties. *Proc. Natl. Acad. Sci. U.S.A.* **2020**, *117*, 820−825.
(40) Li, Y.; Liang, J.; Ding, H.; Lu, J.; Mu, X.; Yan, P.; Zhang, X.; Chen, K.; Li, M.; Persson, P. O. Å.; Hultman, L.; Eklund, P.; Du, S.; Yang, H.; Chai, Z.; Huang, Q. Near-Room Temperature Ferromagnetic Behavior of Single-Atom-Thick 2D Iron in Nanolaminated Ternary MAX Phases. *Appl. Phys. Rev.* **2021**, *8*, 031418.
(41) Chen, L.; Li, Y.; Zhao, B.; Liu, S.; Zhang, H.; Chen, K.; Li, M.; Du, S.; Xiu, F.; Che, R.; Chai, Z.; Huang, Q. Multiprincipal Element M_2FeC (M = Ti,V,Nb,Ta,Zr) MAX Phases with Synergistic Effect of Dielectric and Magnetic Loss. *Adv. Sci.* **2023**, *10*, No. 2206877.
(42) Hamm, C. M.; Dürrschnabel, M.; Molina-Luna, L.; Salikhov, R.; Spoddig, D.; Farle, M.; Wiedwald, U.; Birkel, C. S. Structural, Magnetic and Electrical Transport Properties of Non-Conventionally Prepared MAX Phases V_2AlC and $(V/Mn)_2AlC$. *Mater. Chem. Front.* **2018**, *2*, 483−490.
(43) Caspi, E. N.; Chartier, P.; Porcher, F.; Damay, F.; Cabioc'h, T. Ordering of (Cr,V) Layers in Nanolamellar $(Cr_{0.5}V_{0.5})_{n+1}AlC_n$ Compounds. *Mater. Res. Lett.* **2015**, *3*, 100−106.
(44) Zhou, Y.; Meng, F.; Zhang, J. New MAX-Phase Compounds in the V−Cr−Al−C System. *J. Am. Ceram. Soc.* **2008**, *91*, 1357−1360.
(45) Ebert, H.; Mankovskyy, S.; Freyer, H.; Deng, M. Magnetic Static Response Functions. *J. Phys.: Condens. Matter* **2003**, *15*, S617.
(46) Deng, M.; Freyer, H.; Voitländer, J.; Ebert, H. Relativistic Calculation of Magnetic Linear Response Functions Using the Korringa−Kohn−Rostoker Green's Function Method. *J. Phys.: Condens. Matter* **2001**, *13*, 8551.
(47) Gyorffy, B. L. Coherent-Potential Approximation for a Nonoverlapping-Muffin-Tin-Potential Model of Random Substitutional Alloys. *Phys. Rev. B* **1972**, *5*, 2382−2384.
(48) Shein, I. R.; Ivanovskii, A. L. Structural, Elastic, Electronic Properties and Fermi Surface for Superconducting Mo_2GaC in Comparison with V_2GaC and Nb_2GaC from First Principles. *Physica C* **2010**, *470*, 533−537.
(49) Rahm, M.; Hoffmann, R.; Ashcroft, N. W. Atomic and Ionic Radii of Elements 1−96. *Chem. − Eur. J.* **2016**, *22*, 14625−14632.
(50) Vegard, L. Die Konstitution Der Mischkristalle Und Die Raumfüllung Der Atome. *Z. Phys.* **1921**, *5*, 17−26.
(51) Tong, H.; Lin, S.; Huang, Y.; Tong, P.; Song, W.; Sun, Y. Difference in Physical Properties of MAX-Phase Compounds Cr_2GaC and Cr_2GaN Induced by an Anomalous Structure Change in Cr_2GaN. *Intermetallics* **2019**, *105*, 39−43.
(52) Liu, Z.; Waki, T.; Tabata, Y.; Yuge, K.; Nakamura, H.; Watanabe, I. Magnetic Ground State of the $M_{n+1}AX_n$-Phase Nitride Cr_2GaN. *Phys. Rev. B* **2013**, *88*, No. 134401.
(53) Siebert, J. P.; Bischoff, L.; Lepple, M.; Zintler, A.; Molina-Luna, L.; Wiedwald, U.; Birkel, C. S. Sol-Gel Based Synthesis and Enhanced Processability of MAX Phase Cr_2GaC. *J. Mater. Chem. C* **2019**, *7*, 6034−6040.
(54) Mohn, P. *Magnetism in the Solid State: An Introduction*; Springer Science & Business Media, 2002; Vol. *134*.

https://doi.org/10.1021/acs.chemmater.3c00591
Chem. Mater. 2023, 35, 4427−4434